Progress In Electromagnetics Research B, Vol. 98, 107–123, 2023

Dual Stopband Type NGD Network Design for True Time-Delay Based Multi-Beam Steerer Application

Blaise Ravelo[1, *], Glauco Fontgalland[2], Ana Paula B. Dos Santos[2], Hugerles S. Silva[3, 4], Nour M. Murad[5], Fayrouz Haddad[6], Mathieu Guerin[6], and Wenceslas Rahajandraibe[6]

Abstract—An original application of stopband (SB) type negative group delay (NGD) electronic function is introduced. The unfamiliar SB-NGD circuit is designed with RLC-network lumped passive topology. The SB-NGD circuit is exploited to operate as a true-time delay (TTD) device for smart dual-beam phased array design. The two-port passive topology for designing an SB-NGD circuit constituted by an RLC-network is described. The theory and design method of the employed SB-NGD passive circuit are detailed. The microwave theory of the SB-NGD topology is elaborated from S-matrix modelling. The SB-NGD canonical form is innovatively introduced in function of the expected specifications. The synthesis design equations allowing to determine the R, L, and C component values in function of the NGD specifications are formulated. The SB-NGD behavior is verified by comparison of calculated and simulated S-parameters from two different proofs-of-concept (POC). Illustrative results with a very good agreement showing SB-NGD behavior are observed around the arbitrarily chosen central frequencies $f_1 = 0.7\,\text{GHz}$ and $f_2 = 1\,\text{GHz}$ over a bandwidth of 50 MHz. The design principle of TTD-based smart dual-beam is described. The dual-band SB-NGD circuit is designed to operate as a dual-band TTD device with fixed delays at t_1 (f_1) = 357 ps and t_2 (f_2) = 875 ps, respectively. A radiation pattern showing the smart dual-beam steering operating system at f_1 and f_2 frequencies is discussed.

1. INTRODUCTION

To improve the front-end RF and microwave communication performance, innovative circuit design is necessary [1]. One of the key elements to improve communication performance is based on beam-steering antenna array design [2–4]. Different antenna array topologies [1, 2] have been proposed. But these topologies need to be improved to suppress the radio frequency (RF) impairment in massive antenna arrays [3]. To increase the compactness and linearity, metamaterial-based array antenna innovative topology was proposed [4, 5] by using linear metamaterial-based phase shifters (PSs) [6].

1.1. Brief State of the Art on NGD Microwave Engineering Applications

The elaboration of negative refractive index (NRI) aspect of metamaterial was an inspiration for the emerging RF and microwave function operating with bandpass (BP) type negative group delay (NGD) [7, 8]. Metamaterial BP-NGD circuits were implemented with significantly lossy periodical

Received 9 December 2022, Accepted 3 February 2023, Scheduled 15 February 2023
* Corresponding author: Fayrouz Haddad (fayrouz.haddad@im2np.fr).
[1] School of Electronic & Information Engineering, Nanjing University of Information Science & Technology (NUIST), Nanjing 210044, Jiangsu, China. [2] Applied Electromagnetic and Microwave Lab., Federal University of Campina Grande, Campina Grande/PB, 58429, Brazil. [3] Instituto de Telecomunicações and Departamento de Eletrónica, Telecomunicações e Informática, Universidade de Aveiro, Campus Universitário de Santiago, Aveiro 3810-193, Portugal. [4] Department of Electric Engineering, University of Brasília (UnB), Federal District 70910-900, Brazil. [5] PIMENT, Network and Telecom Lab, Institut Universitaire de Technologie, University of La Reunion, Saint Pierre 97410, France. [6] Aix-Marseille University, CNRS, University of Toulon, IM2NP UMR7334, Marseille 13007, France.

cells [8]. Therefore, RF and microwave engineers wondered about BP-NGD circuit application existence. As the answer from some research groups to such a curious question about the NGD circuit usefulness, tentative applications were suggested [9–27]. A survey on NGD RF and microwave device applications is proposed in [9]. BP-NGD function was introduced for adaptative aspect in a microwave signal processing building block [18]. Then, an NGD circuit was also proposed for the compensation of microwave devices [11, 12]. A remarkable NGD application technique for group delay (GD) equalization [12–14] was introduced. The NGD equalization technique was exploited for the microwave signal RC-interconnects [12], ultra-wideband (UWB) GD effect [13], signal synchronization [14], and also BP filter GD rabbit ear reduction [15]. Unfamiliar BP-NGD circuits were also designed for RF and microwave antenna arrays [16–19]. NGD array antenna technique was, recently, exploited to develop innovative topologies of antenna array operating with squint-free beamforming [18, 19]. This type of NGD antenna array application is fundamentally implemented with non-Foster elements using BP-NGD networks [18–21]. An innovative microwave engineering application was developed for designing broadband phase shifter (PS) using BP-NGD function operating independently of the frequency [22–27]. This concept of NGD PS was also implemented by means of stopband (SB) type NGD circuit [27]. Before the exploration of the SB-NGD circuit application, it is worth to recall the fundamental types and specifications of NGD circuit topologies.

1.2. Recall on the Fundamental Types of NGD Topologies

Recent investigations disclosed by research teams from different worldwide corners [28–54] confirm the diversity of BP-NGD topologies. The BP-NGD effect was verified with diverse microwave structures as absorptive filter [28] and electromagnetic interference (EMI) based techniques [29]. A topology of BP-NGD active circuit was implemented by using microwave transversal filter approach [30]. Due to the complexity, the design of more compact microwave passive circuits was proposed [31, 32]. More extensive microwave function aspects as the dual-band BP-NGD behavior were developed in [33–38]. Dual-band NGD functions were also implemented with compact circuits [36, 37] and with multi-coupled lines [38]. Despite the progressive state of the art on the BP-NGD circuit design, because of the unfamiliarity, curious questions are still raised by RF and microwave design engineers about the interpretation of the NGD effect. For a deep illustration, an analogy between the filter theory and the NGD function theory was addressed in [39, 40]. In contrast with the filter, NGD function focuses mainly on the negative sign associated with the GD response but not the magnitude response [39, 40]. The concept of low-pass (LP) NGD function was proposed with lumped passive, lumped active, via passive, and CMOS integrated circuit (IC) circuits [41–50]. Different types of NGD topologies as high-pass (HP) [51, 52], BP- [28–38], and stopband (SB) [53, 54] NGD RF passive circuits inspired from LP-NGD cell were introduced. Nevertheless, most of the published research works available in the literature on the NGD RF and microwave circuit applications are mainly focused on the BP-NGD function [7–26, 28–38]. However, only one paper is so far available on the SB-NGD circuit application for the stair PS design [27]. Therefore, more investigation is necessary to explore the design ability and potential application of SB-NGD type circuits.

1.3. Novelty and Outline of the Paper

The research on original application of SB-NGD type passive circuit for the smart beam steering design is developed in the present paper. The main items of performed study novelty are:

- The design method of true time delay (TTD) device from SB-NGD circuit synthesis in function of targeted working frequency and delay value.
- The design and capabilities of smart beam steering at the targeted operating frequency by using dual-band SB-NGD circuit.
- The design method of SB-NGD circuit based phased array antenna (PAA) for future transceiver (TxRx) communication system.

For the better comprehension to elaborate this potential application, the paper is organized as follows:

- Section 2 focuses on the theory of SB-NGD function. The S-matrix model is introduced. Then, the SB-NGD canonical form is established in function of the targeted specifications in terms of center frequency, GD value, and bandwidth. The synthesis design equation of circuit in function of the SB-NGD specifications is formulated.
- Section 3 dedicates the discussion on the dual SB-NGD validation. Simulated and calculated results about the SB-NGD aspect from a proof-of-concept (POC) circuit are compared and commented.
- Section 4 investigates the design principle and illustrative results of dual SB-NGD original application as TTD circuit. The relationship analytical investigation on phase shift, beam direction, and the antenna factor (AF) is elaborated. For the feasibility study, a POC of smart beam steering circuit is designed, simulated, and discussed.
- Section 5 is the last conclusion of the paper.

2. DESIGN METHODOLOGY OF THE CONSIDERED SB-NGD CIRCUIT

This section describes the considered SB-NGD circuit theory. After definition of SB-NGD ideal response specifications, the equivalent S-matrix model of an RLC-series network-based cell is presented. Then, the SB-NGD analysis is established.

2.1. Specificities and Basic Definition of SB-NGD Function

Suppose that the SB-NGD microwave circuit is represented by the two-port black box proposed in Fig. 1(a). For the case of symmetrical microwave passive circuits, the analytical equivalent model can be represented by S-matrix:

$$[S(s)] = \begin{bmatrix} S_{11}(s) & S_{21}(s) \\ S_{21}(s) & S_{11}(s) \end{bmatrix} \tag{1}$$

by denoting angular frequency, ω, we have $s = j\omega$ the Laplace variable. The associated transmission phase is defined by $\varphi(\omega) = \arg[S_{21}(j\omega)]$. The corresponding GD response is given by relation $GD(\omega) = -\partial\varphi(\omega)/\partial\omega$. The S-matrix equivalent circuit represented by Equation (1) behaves as NGD function if there is at least an angular frequency, ω, where $GD(\omega) < 0$. The main specificities characterizing the SB-NGD type topology can be understood by the ideal diagrams of Fig. 1(b), Fig. 1(c), and Fig. 1(d).

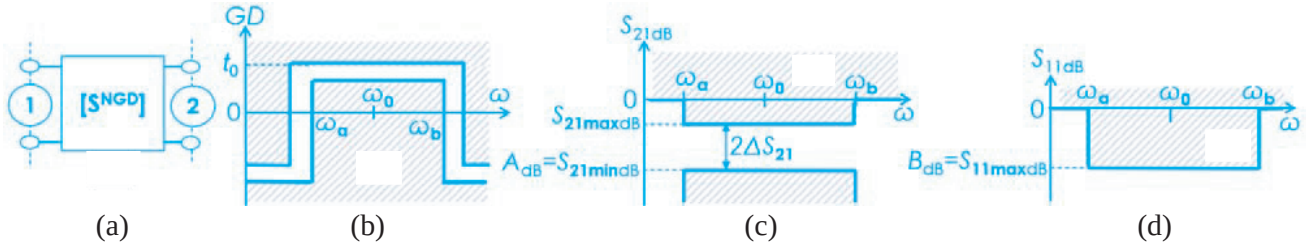

Figure 1. (a) Two-port black box and, (b) GD, (c) S_{21} and (d) S_{11} ideal responses of SB-NGD function.

We can underline from Fig. 1(b) that SB-NGD function can be characterized by:

- The cut-off angular frequencies, ω_a, and ω_b, $(\omega_a < \omega_b)$ as roots of equation $GD(\omega) = 0$.
- The positive GD (PGD) bandwidth (BW) $[\omega_a, \omega_b]$ is defined by $\Delta\omega = \omega_b - \omega_a = 2\pi\Delta f$.
- The SB-NGD mathematical specification associated with the GD diagram is expressed by:

$$\begin{cases} GD(\omega_{a,b}) = 0 \\ GD(\omega \in [\omega_a, \omega_b]) = t_0 > 0 \end{cases}. \tag{2}$$

In addition to the GD responses, in the PGD BW, given real positive parameters $A < 1$ and $B < 1$, the SB-NGD microwave circuit is also specified by:

- The transmission coefficient, as specified in Fig. 1(c), respecting the condition:

$$\begin{cases} S_{21\,\min} = A - \Delta S_{21} \\ S_{21\,\max} = A + \Delta S_{21} \\ S_{21\,\min} \leq S_{21}(\omega \in [\omega_a, \omega_b]) \leq S_{21\,\max} \end{cases}. \tag{3}$$

- And the reflection coefficient, as illustrated by Fig. 1(d), with below the given maximal value, $B = S_{11\,\max}$:

$$S_{11}(\omega \in [\omega_a, \omega_b]) \leq S_{11\,\max}. \tag{4}$$

2.2. *S*-Matrix Model of Lumped RLC-Network Based SB-NGD Cell

The two-port circuit constituted by the RLC-network shown in Fig. 2 represents the topology of SB-NGD circuit under study. We can theorize this passive cell by the elaboration of its S-matrix model which can be established from Y-to-S transform. The equivalent admittance of the RLC-network constituting the circuit depicted by Fig. 2 is given by:

$$\Upsilon(s) = \frac{1}{R} + \frac{Cs}{1 + LCs^2}. \tag{5}$$

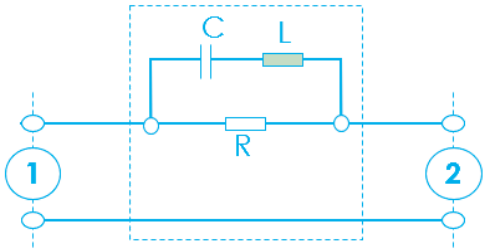

Figure 2. Lumped RLC passive network-based SB-NGD cell under consideration.

Acting as a single element series topology, the associated equivalent admittance matrix is written as:

$$[Y(s)] = \Upsilon(s) \begin{bmatrix} 1 & -1 \\ -1 & 1 \end{bmatrix}. \tag{6}$$

From the following Y-to-S matrix transform, we have:

$$[S(s)] = \left\{ \begin{bmatrix} 1 & 0 \\ 0 & 1 \end{bmatrix} - R_0 [Y(s)] \right\} \times \left\{ \begin{bmatrix} 1 & 0 \\ 0 & 1 \end{bmatrix} + R_0 [Y(s)] \right\}^{-1}. \tag{7}$$

We remind that $R_0 = 50\,\Omega$ represents the terminal reference impedance of the S-parameters. It yields from relationship (7) that the reflection and transmission coefficients of the cell introduced by Fig. 2 are respectively:

$$S_{11}(s) = R\left(LCs^2 + 1\right) / \left[(R + 2R_0)\, LCs^2 + 2R_0RCs + R + 2R_0\right] \tag{8}$$

$$S_{21}(s) = 2R_0\left(LCs^2 + RCs + 1\right) / \left[(R + 2R_0)\, LCs^2 + 2R_0RCs + R + 2R_0\right]. \tag{9}$$

From the last expression, we can formulate the transfer function (TF) canonical form specific to SB-NGD topology.

2.3. SB-NGD Transmission Coefficient Canonical Form

The SB-NGD TF canonical form consists in expressing the transmission coefficients figuring out the key specifications as PGD value $t_0 > 0$, PGD center angular frequency ω_0, and PGD bandwidth. By the identification of polynomial coefficients with the transmission coefficient of Equation (12), the SB-NGD TF canonical form can be formulated as:

$$T(s) = T_n\left(s^2 + \omega_n s + \omega_0^2\right) / \left(s^2 + \omega_d s + \omega_0^2\right). \tag{10}$$

This canonical form is defined by the following real positive coefficients:

$$T_n = 2R_0/(R+2R_0) \tag{11}$$

$$\omega_0 = 1/\sqrt{LC} \tag{12}$$

$$\omega_n = R/L \tag{13}$$

$$\omega_d = 2R_0^R/\left[L\left(2R_0^+R\right)\right]. \tag{14}$$

From the previous expression, the SB-NGD fundamental properties can be analytically examined. Accordingly, we can demonstrate from the GD applied to the phase of transmittance written in Equation (9) that the PGD at the targeted working frequency is equal to:

$$GD(\omega_0) = L/R_0. \tag{15}$$

Furthermore, the PGD bandwidth of the SB-NGD TF canonical form is given by:

$$\Delta\omega = R\sqrt{R_0}\left(\varpi - R\sqrt{R_0C}\right) \Bigg/ \left\{L\sqrt{(2R_0+R)\left[\varpi^2 - 2L(2R_0+R) - R\varpi\sqrt{R_0C}\right]}\right\} \tag{16}$$

with:

$$\varpi = \sqrt{CR_0R + 2L(2R_0+R)}. \tag{17}$$

2.4. SB-NGD Circuit Synthesis and Design Equations

Like the design method introduced in [40, 53, 54], some alternative formulas of SB-NGD circuit R, L and C parameters are determined in the present subsection in function of the targeted specifications.

2.4.1. Synthesis Formulas

The proposed synthesis formulas are elaborated from the previously expressed specifications. The formulas are established by inverting PGD center frequency via the RLC-network resonance frequency given by Equation (12) and the expected PGD written in Equation (15) and the PGD bandwidth written in Equation (16). By solving the design equation, we can determine the R, L, and C parameter equations of the SB-NGD circuit:

$$R = R_0t_0\Delta\omega\left(t_0\Delta\omega + \sqrt{16 + t_0^2\Delta\omega^2}\right)\Big/4 \tag{18}$$

$$L = R_0t_0 \tag{19}$$

$$C = 1/\left(R_0\omega_0^2t_0\right). \tag{20}$$

Numerical applications of these equations permit to calculate the curves of abacuses showing the variation of these parameters versus the range of the targeted SB-NGD characteristics.

2.4.2. Graphical SB-NGD Analysis versus Circuit Parameters

The proposed graphical analysis represents the SB-NGD circuit parameters drawn from these synthesis equations, giving the reference impedance, $R_0 = 50\,\Omega$. The established cartographies of the L, R, and C parameters were plotted in Fig. 3. It can be predicted from Equation (19) that the inductor plotted in Fig. 3(a)= increases linearly with respect to t_0 from $L_{\min} = 5\,\text{nH}$ to $L_{\max} = 500\,\text{nH}$. The resistor varies from $R_{\min} = 31\,\mu\Omega$ to $R_{\max} = 1078\,\Omega$ as shown in Fig. 3(b). The capacitor C varies inversely proportional to the delay and center frequency as seen in Fig. 3(c). The capacitor decreases from 563 nF to 0.6 fF. Acting as a rarely studied NGD type of RF and microwave circuit, it is particularly important to get more insight about the familiarity to perform several analyses about the SB-NGD aspect.

To verify the feasibility of the developed SB-NGD theory, POC investigation will be presented in the next section.

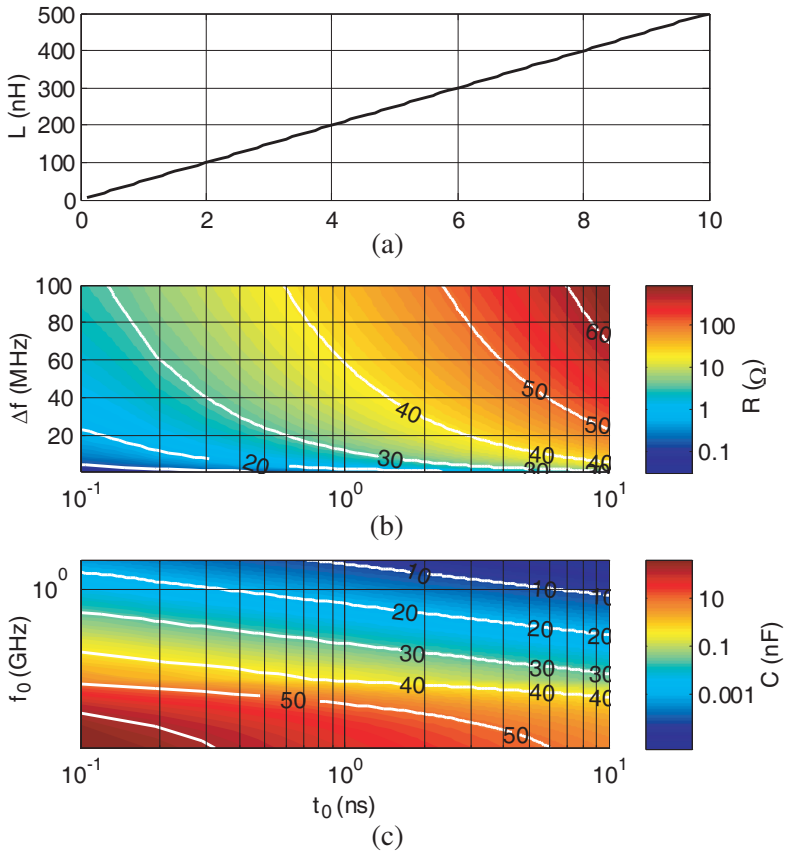

Figure 3. Cartographies of SB-NGD circuit parameters: (a) R versus (t_0, Δf) and (b) L versus (t_0, f_0).

3. ILLUSTRATIVE VALIDATIONS OF THE DUAL SB-NGD BEHAVIOR

The present section confirms the feasibility study of the TTD circuit design of dual SB-NGD behavior of the considered lumped passive topology shown by Fig. 3. After the POC description, parametric simulations are described in order to quantify the influence of the R, L, and C parameters on the NGD behavior. The dual SB-NGD circuit computations for reflection and transmission coefficients were made using Equations (8) and (9) in MATLAB®. Commercial tool simulations were carried out to the analytical calculations.

3.1. Description of the Dual SB-NGD Circuit POC Design

As a concrete case of study, a POC of dual SB-NGD circuit was designed. The POC consists of two different cells of topology introduced earlier in Fig. 3. The constituting cells are intended to operate with center frequencies, $f_1 = 0.7$ GHz for circuit$_1$ and $f_2 = 1$ GHz for circuit$_2$. The design and simulation of the POC circuits are performed by means of design in the schematic environment of ADS® electronic and RF/microwave simulation tools from Keysight technologies®. The synthesis approach was carried out by fixing the delay and BW, the R, L, and C parameters of the dual SB-NGD POC were calculated from formulas (18), (19), and (20). The POC circuit components values were determined with respect to the targeted specifications. The designed lumped circuit parameters are indicated in Table 1. The POCs of SB-NGD circuit were designed as hybrid technology. The design imperfection effects are taken into account for the performed simulation by including the interconnect two-port straight-shape and three-port Tee-shape lines. The POCs are assumed constituted by R, L, and C lumped components implemented on Cu-metalized FR4 dielectric substrate in microstrip technology.

Table 1. Parameters of the POCs represented by SB-NGD circuit$_1$ and circuit$_2$.

POC	Description	Parameters	Values
Circuit$_1$	Center frequency	$f = f_1$	0.7 GHz
	Delay	t_1	357 ps
	BW	$BW_1 = BW$	50 MHz
	Resistor	R_1	5.45 Ω
	Inductor	L_1	17.8 nH
	Capacitor	C_1	2.9 pF
Circuit$_2$	Center frequency	$f = f_2$	1 GHz
	Delay	t_2	875 ps
	BW	BW_2= BW	50 MHz
	Resistor	R_2	12.8 Ω
	Inductor	L_2	43.7 nH
	Capacitor	C_2	0.58 pF

Table 2. Considered POC substrate parameters.

Structure	Description	Parameters	Values
Substrate	Relative permittivity	ε_r	4.5
	Loss tangent	$\tan(\delta)$	0.02
	Thickness	h	1.6 mm
Metallization conductor	Copper conductivity	σ	58 MS/s
	Thickness	t	35 µm
Access and interconnect lines (TL$_{k=1,\ldots,7}$)	Length	d	3 mm
	Width	w	3 mm

The substrate physical characteristics are addressed in Table 2. Accordingly, the circuit schematic of designed and simulated single cell SB-NGD circuit including the microstrip interconnect effects and Tee-ones is introduced in Fig. 4(a). Moreover, Fig. 4(b) represents the ADS® schematic of the two-cell based dual SB-NGD circuit POC. The latter is composed by two different cells, $R_1L_1C_1$ network based circuit$_1$ and $R_2L_2C_2$ network based circuit$_2$. The discussion on comparative results of the designed SB-NGD circuit POCs will be examined in the following subsections.

3.2. Comparison between SB-NGD POC Analytical Calculations and Simulations

The comparison between analytical calculation and commercial tool-based simulation is discussed in the present subsection. To validate the dual SB-NGD behavior, the calculated and simulated GDs and S-parameters are compared within the frequency band defined from $f_{\min} = 0.6$ GHz to $f_{\max} = 1.1$ GHz. Fig. 5 displays the obtained results. The results from the dual SB-NGD POC are also compared to those from circuit$_1$ and circuit$_2$. The results displayed by Fig. 5 represent GD, S_{11}, and S_{21} responses of:

- Simulated circuit$_1$ indicated by "Cir.$_1$", which are plotted in blue sky dashed lines.
- Simulated circuit$_2$ indicated by "Cir.$_2$", which are plotted in navy blue dashed lines.
- Calculated dual SB-NGD circuit POC ("Calc.(POC)") plotted in solid black lines.
- Simulated dual SB-NGD circuit POC ("Simu.(POC)") plotted in solid red lines.

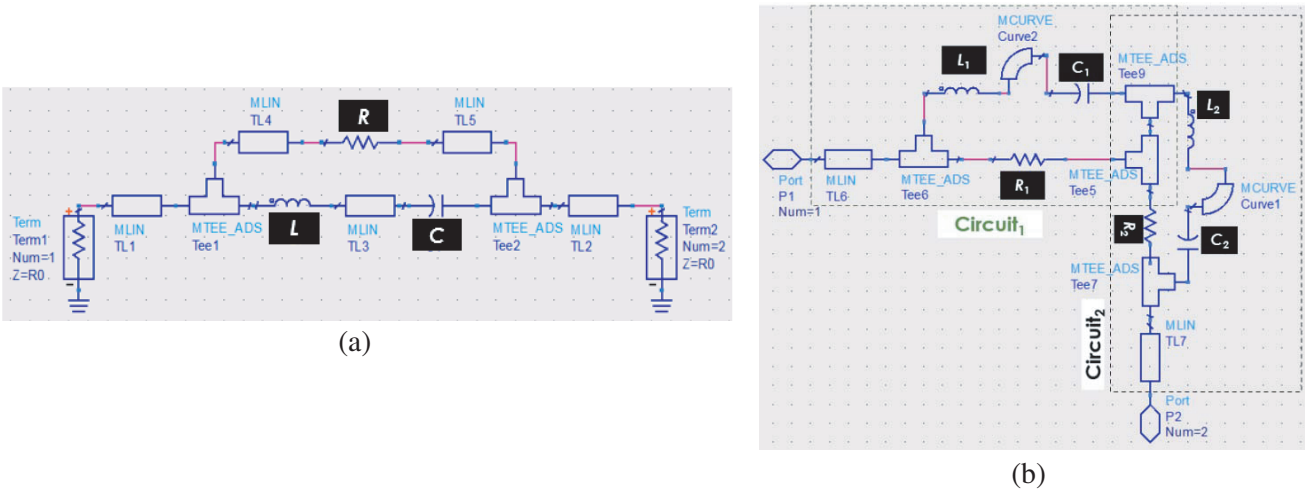

Figure 4. ADS® schematic design of (a) single and (b) dual SB-NGD circuit POC.

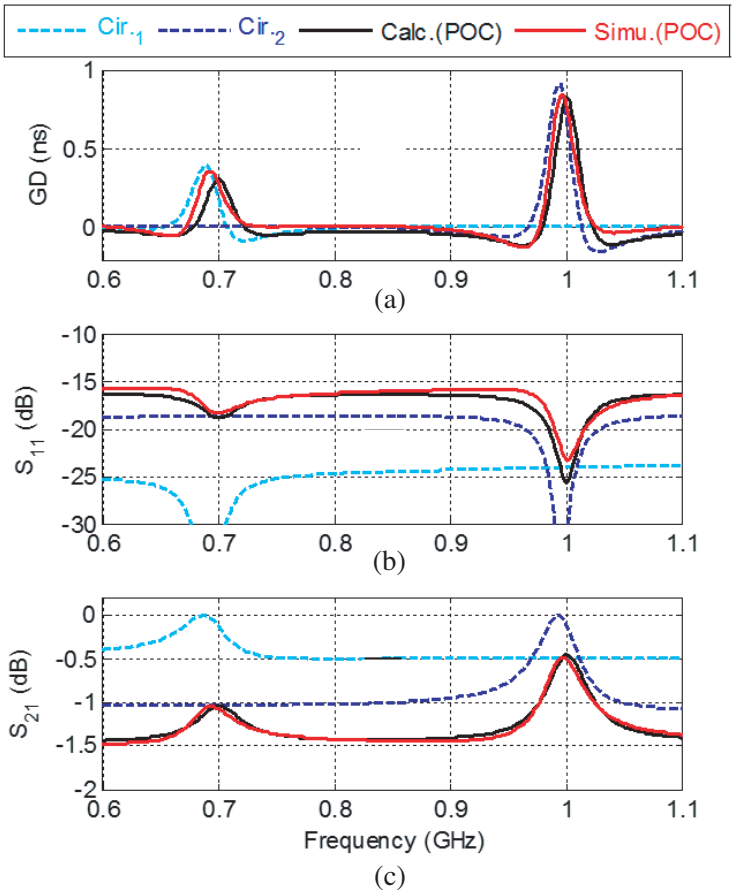

Figure 5. Comparisons of calculated and simulated (a) *GD*, (b) S_{11} and (c) S_{21} of the SB-NGD POCs shown in Fig. 4.

The expected results of GD can be seen in Fig. 5(a). A slight shift of center frequencies appears due to the interconnect effect imperfections. We can remark that the circuit behaves as a dual SB-NGD function with center frequencies about $f_1 = 0.7\,\text{GHz}$ and $f_2 = 1\,\text{GHz}$. The TTDs are equal

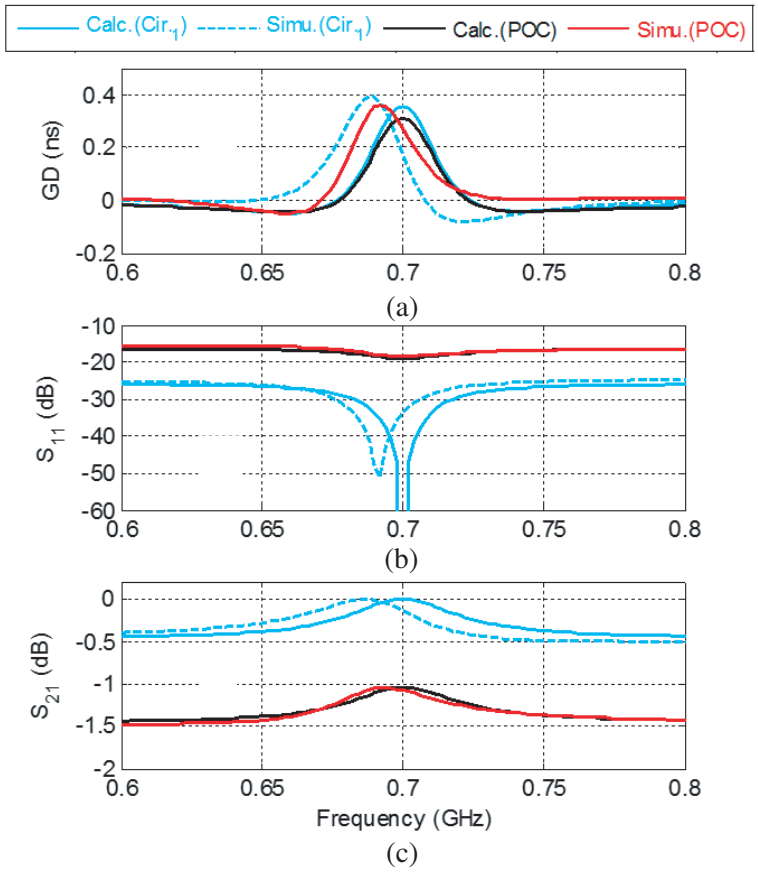

Figure 6. Comparisons of calculated and simulated (a) GD, (b) reflection and (c) transmission parameters from circuit$_1$ and dual SB-NGD POC.

to $\tau_1 = 0.31\,\text{ns}$ and $\tau_2 = 0.82\,\text{ns}$, respectively. As seen in Fig. 5(b), the dual SB NGD circuit losses are more significant. In the dual-band bandwidths, the circuit reflection coefficient is better than $-15\,\text{dB}$. However, the transmission coefficients displayed by Fig. 6(c) are $S_{21}(f_1) \approx -1\,\text{dB}$ and $S_{21}(f_2) \approx -0.5\,\text{dB}$. To confirm the robustness of the SB-NGD function, uncertainty analyses can be performed with respect to the RLC-parameter variabilities.

3.3. Dual SB-Circuit Uncertainty Analyses

The present section investigates the uncertainty effects of dual SB-NGD POC compared circuit$_1$ and circuit$_2$.

3.3.1. Discussion on Calculated and Simulated Results from Circuit$_1$

We remind that circuit$_1$ is intended to operate at center frequency, $f_1 = 0.7\,\text{GHz}$. In this case of analysis, the present S-parameter analysis is carried out from $f_{\min} = 0.6\,\text{GHz}$ to $f_{\max} = 0.8\,\text{GHz}$. We propose GD, S_{11}, and S_{21} comparisons between the calculated ("Calc." plotted in sky blue solid line) and simulated ("Simu." plotted in sky blue dashed line) circuit$_1$ displayed by Fig. 6. The calculated and simulated GDs and S-parameters of circuit$_1$ are also compared to dual SB-NGD circuit results. It can be pointed out that these results present a very good agreement. As expected, in the working frequency band, the tested prototype behaves as an SB-NGD function around center frequency of approximately $f_0 = 0.7\,\text{GHz}$ as seen in Fig. 6(a). It can be seen in Fig. 6(b) and Fig. 6(c) that S_{21} and S_{11} are globally better than $-0.001\,\text{dB}$ and $-40\,\text{dB}$ within the test frequency band, respectively.

To complete the study of circuit$_1$, further analyses on the influence of resistor, inductor, and capacitor uncertainty on the SB-NGD behaviors are examined in the remainder paragraphs of the present subsection.

3.3.2. Discussion on Calculated and Simulated Results from Circuit$_2$

The present SB-NGD aspect analysis is focused on the case of circuit$_2$. The analysis approach is performed in the working frequency band of interest, which is delimited by from $f_{\min} = 0.95\,\text{GHz}$ to $f_{\max} = 1.05\,\text{GHz}$. Like the previous case of circuit$_1$, the present one is essentially focused on the results of calculated ("Calc." plotted in navy blue solid line) and simulated ("Simu." plotted in navy blue dashed line) circuit$_2$. In addition, the GD and S-parameter results from $f_{\min} = 0.95\,\text{GHz}$ to $f_{\max} = 1.1\,\text{GHz}$ are compared to dual SB-NGD circuit results. For the SB-NGD characterization of circuit$_2$, the computation and calculation were performed in the frequency band from 0.95 GHz to 1.1 GHz as displayed in Fig. 7. Once again, the calculated and simulated GD and S-parameters are in very good agreement. As expected, in the working frequency band, the circuit$_2$ POC presents the expected SB-NGD behavior. As can be seen in Fig. 7(a), the center frequency is approximately $f_2 = 1\,\text{GHz}$. Fig. 7(b) and Fig. 7(c) illustrate the good performances of the considered SB-NGD topology in terms of insertion and reflection losses at f_2. The slight frequency shifts of NGD center frequency are mainly due to the model approximation, which we expected to be within the component fabrication tolerance as well. The next section is focused on the original potential application of the SB-NGD circuit under study that has never been done before.

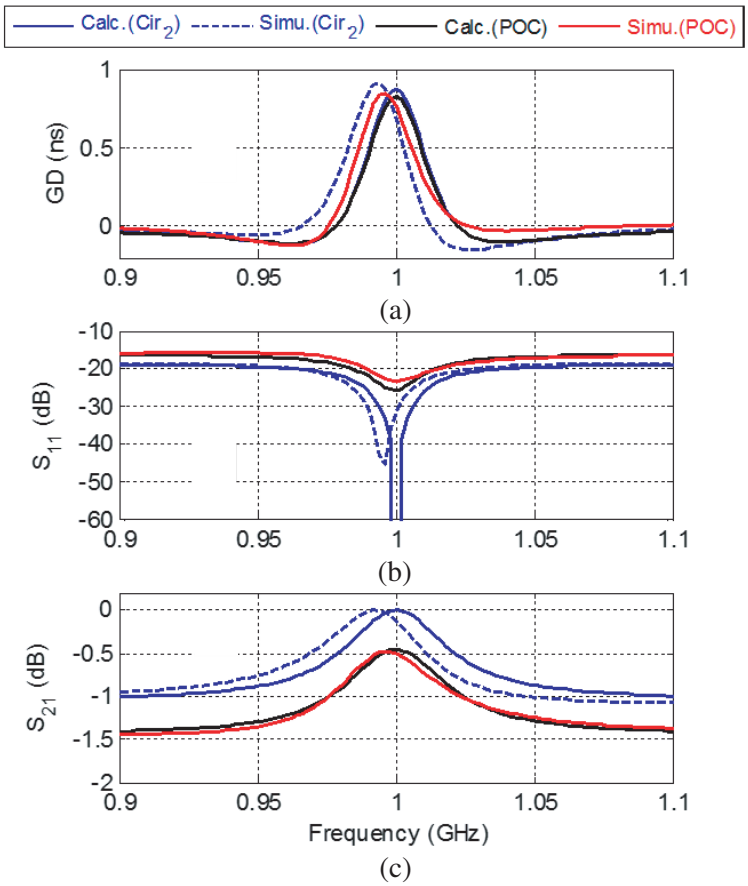

Figure 7. Comparisons of calculated and simulated (a) GD, (b) reflection, and (c) transmission parameters from circuit$_2$ and dual SB-NGD POC.

4. SB-NGD CIRCUIT ORIGINAL APPLICATION FOR SMART DUAL-BEAM STEERING DESIGN

An original application of the SB-NGD circuit for designing RF and microwave front-end system is initiated in the present section. The application idea consists in designing a smart dual-beam steerer working in dual-band frequency. The design principle of the SB-NGD based beam steering is introduced in the following subsection by considering a phased array antenna (PAA).

4.1. Design Principle of Smart Beam Steerer Based on the Use of Dual SB-NGD Circuit

As stated in the previous section, a dual-band TTD circuit can be designed by using dual SB-NGD topology. The introduction of TTD in the PAA system enables to originally generate the smart beam steering capability.

Figure 8 represents the schematic solution of the multi-beam steerer integrating the SB-NGD circuit based PAA. The transmitter (Tx) front-end consists of two terminal branches, in left, $Antenna_l$, and in right, $Antenna_r$ with physical distance d. During the design, we should choose this distance widely lower that the wavelengths associated with the working frequencies, f_m, with $m = \{1, 2\}$ $d \ll \lambda_m = c/f_m$. The scenario configuration with two different orientation beams is illustrated by Fig. 8. The main objective of the SB-NGD based PAA design is to generate beams oriented in the targeted direction in function of frequencies $Beam$ $(f_{m=1,2})$. The beam orientations correspond to azimuthal angles $\theta_m = \theta(f_m)$. The right terminal branch integrates SB-NGD circuit. By hypothesis, the antenna system is expected to simultaneously radiate dual beams free of EMI.

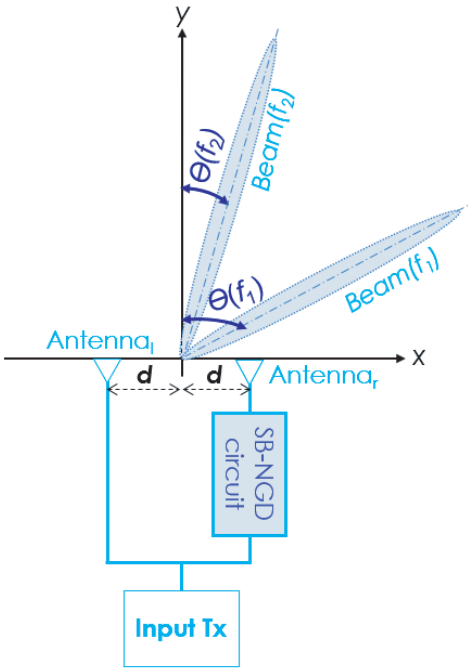

Figure 8. Illustrative scenario of SB-NGD circuit based front-end beam steerer.

4.2. AF versus Beam Direction

For the reason of comprehension, we choose the simple case of PAA constituted by linear array antennas with the number of antenna elements $n = 2$. We can denote the phase shift of SB-NGD TTD at the working frequency, f_m, with $m = \{1, 2\}$ by $\varphi_m = \varphi(f_{m=1,2})$. Consequently, the AF is defined in function of phase shift and beam orientation angle $AF_m(\theta) = AF(f_m, \varphi_m, \theta)$. Based on the PAA theory [55],

the AF can be formulated by:

$$AF_m(\theta) = \sin\left[n \cdot \phi_m(\theta)\right] / \left\{n \sin\left[\phi_m(\theta)\right]\right\} \tag{21}$$

where the phase argument expressed in degree (°) is formulated by:

$$\phi_m(\theta) = \left[720 f_m d \sin(\theta) - \varphi_m c\right] / (2c) \tag{22}$$

and $c = 3 \cdot 10^8$ m/s is the speed of light in the vacuum. The design method of SB-NGD circuit constituting the TTD is expected by targeting $AF_m(\theta = \theta_m) = 1$. The TTD SB-NGD is specified in order to operate with AF verifying Equation (22). Consequently, it yields $\phi_m(\theta = \theta_m) = 0$. By means of formula (22), we should have the relationship between the TTD phase shift and the beam directivity orientation angle expressed in degree (°):

$$\varphi_m = 720 f_m d \sin(\theta_m)/c. \tag{23}$$

The cartographies of Fig. 9 highlight how the phase shift should be defined in function of pair (frequency, beam direction) and (distance, beam direction). We can understand from cartography of Fig. 9(b) that it is better to keep d significantly lower than the wavelength. The design approach of the corresponding SB-NGD circuit specification will be developed in the next subsection.

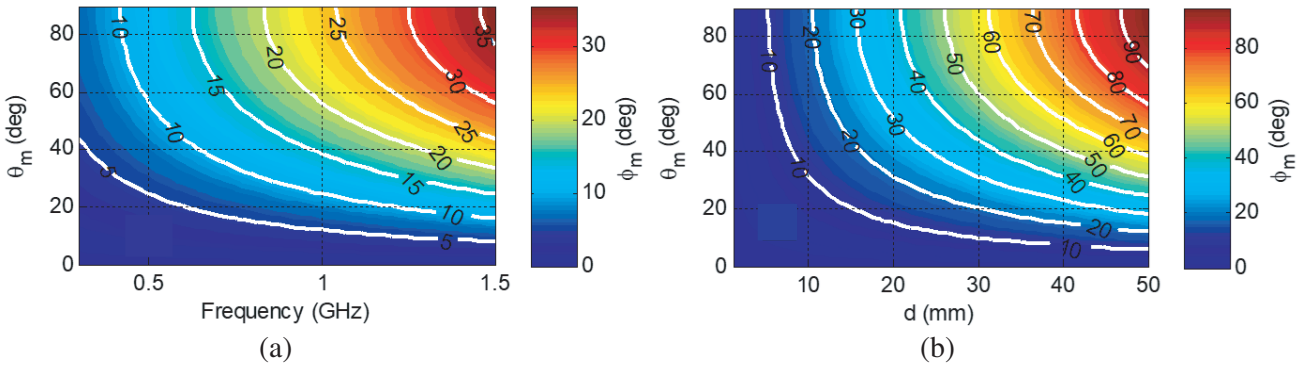

Figure 9. Cartography of phase shift versus pair (a) (f_m, θ_m) and (b) (d, θ_m).

4.3. TTD SB-NGD Specification for Optimal Beam Direction

As aforementioned in Subsection 2.1, the SB-NGD circuit operates as a TTD device when focusing in the PGD bandwidth. Such a particular property can be exploited to design the previously introduced multi-beam PAA. Fig. 10(a) illustrates the desired GD ideal response with two center angular frequencies $f_{m=1,2}$. We suppose that the PGD bandwidths are identical to $\Delta f_1 = \Delta f_2 = \Delta f$. Like all classical microwave devices, we should have good matching and low attenuation losses in the operating frequency bands. Accordingly, Fig. 10(b) and Fig. 10(c) depict the ideal behavior of the dual SB-NGD circuit reflection and transmission coefficients, respectively.

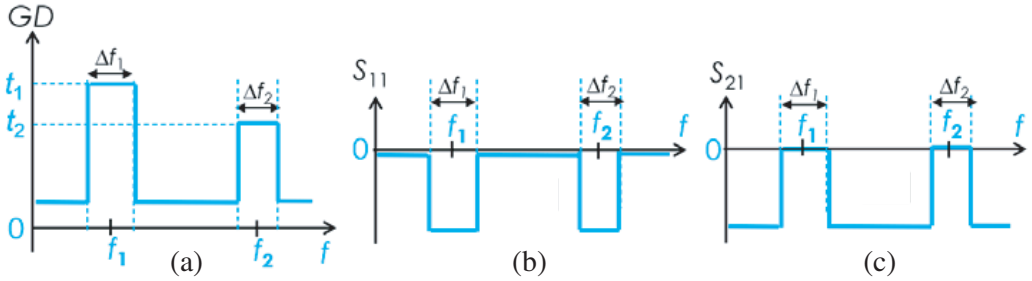

Figure 10. Ideal behavior of dual SB-NGD circuit: (a) *GD*, (b) S_{11}, and (c) S_{21}.

We suppose that the PGD bandwidths are identically equal, and the PGD values are $t_{m=1,2} = GD(f_m)$. At the specific operating frequencies $f_{m=1,2}$, the phase shift associated with the TTDs is given by:

$$\varphi_{m=1,2} = 360(1 - f_m t_m). \tag{24}$$

Substituting the phase shift expressed in Equation (23) into the previous equation, we have:

$$t_m = [c - 2f_m d\sin(\theta_m)]/(f_m c) \tag{25}$$

The next subsection discusses the preliminary result by highlighting the SB-NGD TTD based smart beam steering feasibility.

4.4. Preliminary Result of Dual-Beam Steering at Dual-Band SB-NGD Operating Frequencies

As preliminary insight on the feasibility study of the dual-beam steering, we have considered the schematic of PAA with two directive antennas introduced in Fig. 9. An ideal antenna operating from 0.6 GHz to 1.1 GHz is considered. After analytical computation, we obtain the normalized radiation patterns (black solid curve for $f_1 = 0.7$ GHz and red dashed curve for $f_2 = 1$ GHz) displayed in rectangular plot and semi-logarithmic scale of Fig. 11(a). For a better illustration on the geometrical orientation, the radiation directions can be understood in polar plot of Fig. 11(b). It can be emphasized that as expected, the radiation patterns present different directivities defined by angles:

- $e(f_1) \approx 270°$ at the first operating frequency $f_1 \approx 0.7$ GHz,
- $e(f_2) \approx 45°$ at the second operating frequency $f_2 \approx 1$ GHz.

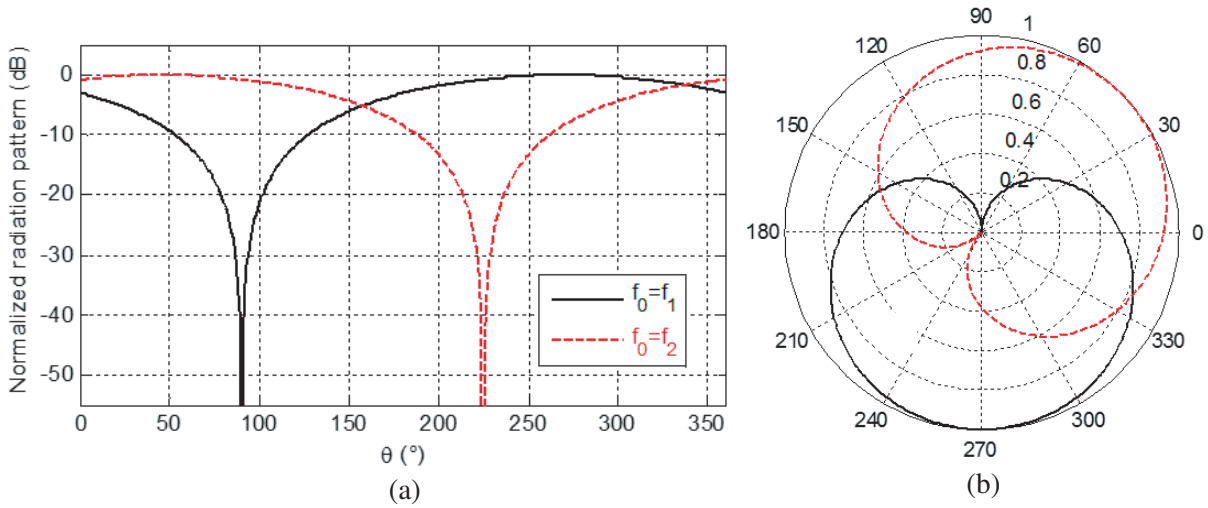

Figure 11. (a) Rectangular and (b) polar plots of normalized radiation patterns at center frequencies, f_1 and f_2.

It is noteworthy that SB-NGD function-based beam steerer is able to communicate simultaneously with two transmission beams oriented in different directions without EMIs.

5. CONCLUSION

So far, most of available NGD circuit designs are focused on LP- and BP-NGD types. The usefulness of other types as SB-NGD topologies remains an open question. The present work explores a potential original RF and microwave engineering application of unfamiliar SB-NGD circuit for a smart beam steered design. The SB-NGD analysis of RLC-lumped network topology is elaborated from the S-parameter modelling by means of transmission coefficient canonical form. The SB-NGD characterization

and property are analytically developed. The synthesis equations allowing to determine the parameters, R, L, and C in function of the targeted specifications are formulated. Two different POCs of SB-NGD circuit working at two different frequencies $f_1 = 0.7\,\text{GHz}$ and $f_2 = 1\,\text{GHz}$ are designed. It was emphasized that the SB-NGD performance depends essentially on the reactive elements, L and C. The SB-NGD circuit is originally exploited to design a beam steerer with PAA-based operation principle description. A beam steerer using the dual SB-NGD circuit working simultaneously at f_1 and f_2 is designed. The proposed original application is illustrated by the analysis of radiation pattern showing the smart dual-beam steering. In the continuation of the present research work, we are intending to develop more practical RF and microwave NGD engineering applications: (i) an experimental study of multi-band NGD circuit-based beam steerer with prototyping is in progress, and (b) realistic environment tests of NGD circuit based PAA for wireless communication technology are also forecasted. By using the NGD antenna design, we have also a perspective study on the improvement of future RF and microwave wireless performance for mobile devices.

ACKNOWLEDGMENT

This research work was supported in part by FCT/MCTES through national funds and, when applicable, co-funded by the EU funds under the project UIDB/50008/2020-UIDP/50008/2020. This research work was also supported in part by NSFC under Grant 61971230, and in part by the Jiangsu Specially Appointed Professor program and Six Major Talents Summit of Jiangsu Province (2019-DZXX-022), and in part by the Startup Foundation for Introducing Talent of Nanjing University of Information Science & Technology (NUIST).

REFERENCES

1. Kallnichev, V., "Analysis of beam-steering and directive characteristics of adaptive antenna arrays for mobile communications," *IEEE Antennas and Propagation Magazine*, Vol. 43, No. 3, 145–152, Jun. 2001.
2. Yan, S.-H. and T.-H. Chu, "A beam-steering and -switching antenna array using a coupled phase-locked loop array," *IEEE Transactions on Antennas and Propagation*, Vol. 57, No. 3, 638–644, Mar. 2009.
3. Hakkarainen, A., J. Werner, K. R. Dandekar, and M. Valkama, "Widely-linear beamforming and RF impairment suppression in massive antenna arrays," *Journal of Communications and Networks*, Vol. 15, No. 4, 383–397, Aug. 2013.
4. Li, Y., M. F. Iskander, Z. Zhang, and Z. Feng, "A new low cost leaky wave coplanar waveguide continuous transverse stub antenna array using metamaterial-based phase shifters for beam steering," *IEEE Transactions on Antennas and Propagation*, Vol. 61, No. 7, 2619–2625, Jul. 2013.
5. Oh, S. S. and L. Shafai, "Compensated circuit with characteristics of lossless double negative materials and its application to array antennas," *IET Microw. Antennas Propag.*, Vol. 1, No. 1, 29–38, 2007.
6. Antoniades, M. A. and G. V. Eleftheriades, "Compact linear lead/lag metamaterial phase shifters for broadband applications," *IEEE Antennas Wireless Propag. Lett.*, Vol. 2, 103–106, 2003.
7. Eleftheriades, G. V., O. Siddiqui, and A. K. Iyer, "Transmission line for negative refractive index media and associated implementations without excess resonators," *IEEE Microw. Wireless Compon. Lett.*, Vol. 13, No. 2, 51–53, Feb. 2003.
8. Siddiqui, O. F., M. Mojahedi, and G. V. Eleftheriades, "Periodically loaded transmission line with effective negative refractive index and negative group velocity," *IEEE Transactions on Antennas and Propagation*, Vol. 51, No. 10, 2619–2625, Oct. 2003.
9. Xiao, J.-K., Q.-F. Wang, and J.-G. Ma, "Negative group delay circuits and applications: Feedforward amplifiers, phased-array antennas, constant phase shifters, non-foster elements, interconnection equalization, and power dividers," *IEEE Microwave Magazine*, Vol. 22, No. 2, 16–32, Feb. 2021.

10. Lucyszyn, S. and I. D. Robertson, "Analog reflection topology building blocks for adaptive microwave signal processing applications," *IEEE Trans. Microw. Theory Techn.*, Vol. 43, No. 3, 601–611, Mar. 1995.
11. Broomfield, C. D. and J. K. A. Everard, "Broadband negative group delay networks for compensation of oscillators, filters and communication systems," *Electron. Lett.*, Vol. 36, No. 23, 1931–1933, Nov. 2000.
12. Ravelo, B., S. Lalléchère, A. Thakur, A. Saini, and P. Thakur, "Theory and circuit modelling of baseband and modulated signal delay compensations with low- and band-pass NGD effects," *Int. J. Electron. Commun.*, Vol. 70, No. 9, 1122–1127, Sept. 2016.
13. Ahn, K.-P., R. Ishikawa, and K. Honjo, "Group delay equalized UWB InGaP/GaAs HBT MMIC amplifier using negative group delay circuits," *IEEE Trans. Microw. Theory Techn.*, Vol. 57, No. 9, 2139–2147, Sept. 2009.
14. Lalléchère, S., L. Rajaoarisoa, L. Clavier, R. S. Galan, and B. Ravelo, "Bandpass NGD function design for 5G microwave signal delay synchronization application," *Comptes Rendus Physique (CRAS)*, Tome 22, No. S1, 53–71, 2021.
15. Shao, T., Z. Wang, S. Fang, H. Liu, and Z. Chen, "A full-passband linear-phase band-pass filter equalized with negative group delay circuits," *IEEE Access*, Vol. 8, 43336–43343, Feb. 2020.
16. Alomar, W. and A. Mortazawi, "Method of generating negative group delay in phase arrays without using lossy circuits," *Proc. IEEE Int. Wireless Symp. (IWS) 2013*, 1–4, Beijing, China, Apr. 14–18, 2013.
17. Alomar, W. and A. Mortazawi, "Elimination of beam squint in uniformly excited serially fed antenna arrays using negative group delay circuits," *Proc. IEEE Int. Symp. Antennas Propag.*, 1–2, Chicago, IL, USA, Jul. 2012.
18. Mirzaei, H. and G. V. Eleftheriades, "Arbitrary-angle squint-free beamforming in series-fed antenna arrays using non-foster elements synthesized by negative-group-delay networks," *IEEE Transactions on Antennas and Propagation*, Vol. 63, No. 5, 1997–2010, May 2015.
19. Zhu, M. and C.-T. M. Wu, "Reconfigurable series feed network for squint-free antenna beamforming using distributed amplifier-based negative group delay circuit," *Proc. 2019 49th European Microwave Conference (EuMC)*, 256–259, Paris, France, Oct. 1–3, 2019.
20. Mirzaei, H. and G. V. Eleftheriades, "Realizing non-Foster reactive elements using negative-group-delay networks," *IEEE Trans. Microw. Theory Techn.*, Vol. 61, No. 12, 4322–4332, Dec. 2013.
21. Zhang, T., R. Xu, and C. M. Wu, "Unconditionally stable non-Foster element using active transversal-filter-based negative group delay circuit," *IEEE Microw. Wireless Compon. Lett.*, Vol. 27, No. 10, 921–923, Oct. 2017.
22. Ravelo, B., M. Le Roy, and A. Perennec, "Application of negative group delay active circuits to the design of broadband and constant phase shifters," *Microwave and Optical Technology Letters*, Vol. 50, No. 12, 3077–3080, Dec. 2008.
23. Ravelo, B., A. Perennec, and M. Le Roy, "Synthesis of frequency-independent phase shifters using negative group delay active circuit," *Int. J. RFMiCAE*, Vol. 21, No. 1, 17–24, Jan. 2011.
24. Ravelo, B., "Distributed NGD active circuit for RF-microwave communication," *Int. J. Electron. Commun.*, Vol. 68, No. 4, 282–290, Apr. 2014.
25. Nebhen, J. and B. Ravelo, "Innovative microwave design of frequency-independent passive phase shifter with LCL-network and bandpass NGD circuit," *Progress In Electromagnetics Research C*, Vol. 109, 187–203, 2021.
26. Meng, Y., Z. Wang, S.-J. Fang, and H. Liu, "Broadband phase shifter with constant phase based on negative group delay circuit," *Progress In Electromagnetics Research Letters*, Vol. 103, 161–169, 2022.
27. Ravelo, B., G. Fontgalland, H. S. Silva, J. Nebhen, W. Rahajandraibe, M. Guerin, G. Chan, and F. Wan, "Original application of stop-band negative group delay microwave passive circuit for two-step stair phase shifter designing," *IEEE Access*, Vol. 10, No. 1, 1493–1508, 2022.

28. Qiu, L.-F., L.-S. Wu, W.-Y. Yin, and J.-F. Mao, "Absorptive bandstop filter with prescribed negative group delay and bandwidth," *IEEE Microw. Wireless Compon. Lett.*, Vol. 27, No. 7, 639–641, Jul. 2017.
29. Wang, Z., Y. Cao, T. Shao, S. Fang, and Y. Liu, "A negative group delay microwave circuit based on signal interference techniques," *IEEE Microw. Wireless Compon. Lett.*, Vol. 28, No. 4, 290–292, Apr. 2018.
30. Wu, C.-T.-M. and T. Itoh, "Maximally flat negative group-delay circuit: A microwave transversal filter approach," *IEEE Trans. Microw. Theory Techn.*, Vol. 62, No. 6, 1330–1342, Jun. 2014.
31. Liu, G. and J. Xu, "Compact transmission-type negative group delay circuit with low attenuation," *Electron. Lett.*, Vol. 53, No. 7, 476–478, Mar. 2017.
32. Shao, T., Z. Wang, S. Fang, H. Liu, and S. Fu, "A compact transmission line self-matched negative group delay microwave circuit," *IEEE Access*, Vol. 5. 22836–22843, Oct. 2017.
33. Ravelo, B. and S. De Blasi, "An FET-based microwave active circuit with dual-band negative group delay," *JMOe*, Vol. 10, No. 2, 355–366, Dec. 2011.
34. Ravelo, B., "Innovative theory on multiband negative group delay topology based on feedback loop power combiner," *IEEE Tran. CAS II: Express Briefs*, Vol. 63, No. 8, 738–742, Aug. 2016.
35. Choi, H., Y. Jeong, J. Lim, S. Y. Eom, and Y. B. Jung, "A novel design for a dual-band negative group delay circuit," *IEEE Microw. Wireless Compon. Lett.*, Vol. 21, No. 1, 19–21, Jan. 2011.
36. Chaudhary, G., Y. Jeong, and J. Lim, "Miniaturized dual-band negative group delay circuit using dual-plane defected structures," *IEEE Microwave Wireless Compon. Lett.*, Vol. 21, No. 1, 19–21, Jan. 2011.
37. Shao, T., S. Fang, Z. Wang, and H. Liu, "A compact dual-band negative group delay microwave circuit," *Radio Engineering*, Vol. 27, No. 4, 1070–1076, Dec. 2018.
38. Zhou, X., B. Li, N. Li, B. Ravelo, X. Hu, Q. Ji, F. Wan, and G. Fontgalland, "Analytical design of dual-band negative group delay circuit with multi-coupled lines," *IEEE Access*, Vol. 8, No. 1, 72749–72756, Apr. 2020.
39. Ravelo, B., "Similitude between the NGD function and filter gain behaviours," *Int. J. Circ. Theor. Appl.*, Vol. 42, No. 10, 1016–1032, Oct. 2014.
40. Ravelo, B., "On the low-pass, high-pass, bandpass and stop-band NGD RF passive circuits," *URSI Radio Science Bulletin*, Vol. 2017, No. 363, 10–27, Dec. 2017.
41. Ravelo, B., "First-order low-pass negative group delay passive topology," *Electronics Letters*, Vol. 52, No. 2, 124–126, Jan. 2016.
42. Ravelo, B., "Demonstration of negative signal delay with short-duration transient pulse," *Eur. Phys. J. Appl. Phys. (EPJAP)*, Vol. 55, No. 10103, 1–8, 2011.
43. Ravelo, B., "Baseband NGD circuit with RF amplifier," *Electronic Letters*, Vol. 47, No. 13, 752–754, Jun. 2011.
44. Ravelo, B., "Methodology of elementary negative group delay active topologies identification," *IET Circuits Devices Syst. (CDS)*, Vol. 7, No. 3, 105–113, May 2013.
45. Ravelo, B., "Theory on negative time delay looped system," *IET Circuits, Devices & Systems*, Vol. 12, No. 2, 175–181, Mar. 2018.
46. Randriatsiferana, R., Y. Gan, F. Wan, W. Rahajandraibe, R. Vauché, N. M. Murad, and B. Ravelo, "Study and experimentation of a 6-dB attenuation low-pass NGD circuit," *Analog. Integr. Circ. Sig. Process.*, Vol. 110, 105–114, 2022.
47. Wan, F., Z. Yuan, B. Ravelo, J. Ge, and W. Rahajandraibe, "Low-pass NGD voice signal sensoring with passive circuit," *IEEE Sensors Journal*, Vol. 20, No. 12, 6762–6775, Jun. 2020.
48. Ravelo, B., F. Wan, S. Lalléchère, W. Rahajandraibe, P. Thakur, and A. Thakur, "Innovative theory of low-pass NGD via-hole-ground circuit," *IEEE Access*, Vol. 8, No. 1, 130172–130182, Jul. 2020.
49. Ravelo, B., W. Rahajandraibe, M. Guerin, B. Agnus, P. Thakur, and A. Thakur, "130-nm BiCMOS design of low-pass negative group delay integrated RL-circuit," *Int. J. Circ. Theor. Appl.*, 1–17, Feb. 2022.

50. Wan, F., T. Gu, B. Li, B. Li, W. Rahajandraibe, M. Guerin, S. Lalléchère, and B. Ravelo, "Design and experimentation of inductorless low-pass NGD integrated circuit in 180-nm CMOS technology," *IEEE Tran. CADICS*, Vol. 41, No. 11, 4965–4974, 2022.
51. Wan, F., X. Huang, K. Gorshkov, B. Tishchuk, X. Hu, G. Chan, F. E. Sahoa, S. Baccar, M. Guerin, W. Rahajandraibe, and B. Ravelo, "High-pass NGD characterization of resistive-inductive network based low-frequency circuit," *COMPEL — The Int. J. Computation and Math. in Elec. and Electron. Eng.*, Vol. 40, No. 5, 1032–1049, 2021.
52. Yang, R., X. Zhou, S. S. Yazdani, E. Sambatra, F. Wan, S. Lalléchère, and B. Ravelo, "Analysis, design and experimentation of high-pass negative group delay lumped circuit," *Circuit World*, 1–25, 2021.
53. Guerin, M., Y. Liu, A. Douyère, G. Chan, F. Wan, S. Lalléchère, W. Rahajandraibe, and B. Ravelo, "Design and synthesis of inductorless passive cell operating as stop-band negative group delay function," *IEEE Access*, Vol. 9, No. 1, 100141–100153, Jul. 2021.
54. Fenni, S., F. Haddad, K. Gorshkov, B. Tishchuk, A. Jaomiary, F. Marty, G. Chan, M. Guerin, W. Rahajandraibe, and B. Ravelo, "AC low-frequency characterization of stop-band negative group delay circuit," *Progress In Electromagnetics Research C*, Vol. 115, 261–276, 2021.
55. Balanis, C. A., *Antenna Theory: Analysis and Design*, 3rd Edition, Wiley, New-York, USA, 2005.